UDK 533.6.011.6

WILDFIRE PROPAGATION: A TWO-DIMENSIONAL MULTIPHASE APPROACH

B. Porterie, D. Morvan*, M. Larini, J. C. Loraud

Institut Universitaire des Systèmes Thermiques Industriels, Marseille, France
* Institut de Recherches sur les Phénomènes Hors Equilibre, Marseille, France

This paper describes a multiphase approach for determining the rate of propagation of a line fire through a randomly-packed fuel bed of thermally-thin cellulosic particles and the induced hydrodynamics inside and above the litter. A set of time-dependent balance equations are solved for each phase (a gas phase and N solid phases) and the coupling between the gas phase and the solid phases is rendered through exchange terms of mass due to the thermal degradation of the fuel material (heating, drying, pyrolysis, and char combustion), momentum, and energy. The radiative transfer equation in the fuel bed is deduced from the P1-approximation, and radiation from the flame to the fuel bed is accounted for with the help of the empirical model of Markstein. Kinetics is incorporated to describe pyrolysis and combustion processes. The solution is performed numerically by a finite-volume method. The development of a line fire from the moment of initiation to quasi-steady propagation is predicted and discussed. Results obtained by this multiphase model are compared to measurements made on laboratory fires using dead pine needles as fuel. The predicted rates of fire spread for some configurations including slope effects agree well with measured values.

1. INTRODUCTION

The present study is concerned with the simulation of wildfires propagating through a fuel bed by using a multiphase mathematical model. Attention is focused on the development of a realistic representation of most of the complex physical and chemical processes that occur in a wildfire in relation to the processes of heating, drying, and pyrolysis of fuel material, and char combustion as well as homogeneous combustion in the gas phase. At this stage of development, a two-dimensional model is formulated for the idealized representation of line fire propagation normal to its span-wise extension. In two dimensions (x, y), line fire propagation can be illustrated by the sketch shown in Fig. 1. The main problem of predicting the rate of propagation of wildfire can be expressed in terms of finding the rate of translation of the ignition interface separating the burning zone and the unburnt fuel [1].

In the present approach, which falls within the framework of the novel formulation of Grishin [2], wildland fire is considered as a multiphase, reactive, and radiative flow. A gas-phase flows through N solid phases which constitute an idealized reproduction of the heterogeneous combustible medium. Each solid phase consists of fuel particles having similar characteristics (physical properties and geometrical aspect). A set of time-dependent equations are obtained for each phase, and the coupling between the gas phase and the N solid phases is rendered through exchange terms of mass, momentum, and energy. The basis of the general multiphase formulation have been given by Larini et al. [3]. The potentiality of the multiphase model has been shown through the use of a simplified 1D model in which some physical phenomena (such as char combustion, diffusion terms) are neglected. In the framework of this simplified model, reverse and forward one-dimensional fire propagations through a heterogeneous medium composed of fixed fuel particles

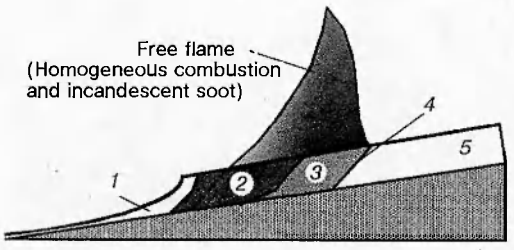

Fig. 1. The physical problem of predicting the rate of propagation of a line fire through a fuel bed:
1 — ash, *2* — burning embers (heterogeneous char combustion), *3* — burning zone of intense pyrolysis, homogeneous and heterogeneous combustion, *4* — ignition interface, *5* — unburnt heated fuel (slow pyrolysis)

have been studied numerically.

Following the classification of Weber [4], previous models of fire spread through a fuel bed can be classified as statistical, empirical, and physical models according to whether they involve no physics at all, no distinction between different modes of heat tranfer (conduction, convection, and radiation), or account for each mechanisms of heat transfer individually. The purpose of these models is restricted to the prediction of the rate of fire propagation. The reader is encouraged to consult the paper of Weber [4] for a complete analysis and an objective comparison of these different models. Among the physical models, the model of Grishin et al. [5] is the first model that incorporates kinetics to describe pyrolysis and combustion, but it does not account for hydrodynamics.

A new development of physical models appeared in 1985 with the pioneering work of Grishin et al. [2], insofar as they describe the hydrodynamics through the fuel matrix and above the fuel bed by using a multiphase approach. These models can predict not only the rate of fire propagation but also its complete behavior. In the work of Grishin et al. [2], thermal equilibrium between two phases (a gas phase and one solid phase) is assumed and the equations are averaged over the height of the forest canopy to simplify the formulation of the general problem.

The aim of the present paper is to propose an extension of the formulation of Grishin et al. [2] to a medium in which a gas phase and N solid phases in thermal nonequilibrium are treated individually. It should allow to demonstrate the ability of the time-dependent multiphase model in predicting the propagation of a line fire through a bed of pine needles and to investigate the physical realism of results obtained for some configurations including slope effects.

2. MULTIPHASE FORMULATION

A complete description of the multiphase formulation for the derivation of governing equations is given by Larini et al. [3]. A brief description is given below.

In the present approach, the fuel bed is considered as a heterogeneous medium composed of solid particles of various kinds. In a small control volume V, N solid phases coexist with the gas phase. Fig. 2 shows an example of a multiphase medium with three types of fuel and a gas phase. Each solid phase consists of particles of the same geometrical (e. g., shape, size, and arrangement)

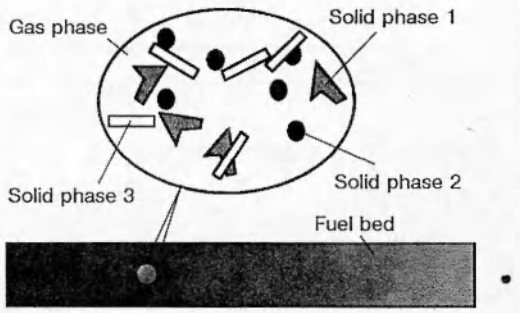

Fig. 2. Example of multiphase medium with three types of fuel and a gas phase

and thermochemical properties providing in this way the same behavior under fire.

The packing ratio of the phase k is defined as $\alpha_k = V_k/V$, where V_k is the volume occupied by the phase k in volume V.

In the same way, the fractional porosity, also named void fraction or "aeration degree", is defined as $\alpha_g = V_g/V$.

From these definitions, we have

$$\alpha_g + \sum_{k=1}^{N} \alpha_k = 1. \tag{1}$$

Transfers between the gas phase and each of the solid phases are the key concept for the understanding of fire propagation mechanisms. These transfers are directly related to the specific wetted area A_k, expressed as follows:

$$A_k = \tilde{n}_k s_k = V_k \frac{\tilde{n}_k s_k}{V_k} = \frac{V_k}{V}\frac{s_k}{v_k} = \alpha_k \sigma_k, \tag{2}$$

where for a phase k, $\sigma_k = s_k/v_k$ is the surface-to-volume ratio of a solid particle, and $\tilde{n}_k$ the number density (number of particles per unit volume).

For each phase (gas phase and N solid phases), a set of time-dependent equations based on the laws of conservation of mass, momentum, chemical species, and energy is considered. The radiative contribution in the energy equation is evaluated by solving the equation of radiative transfer equation.

The derivation is carried out in two steps. In the first step, a small control volume containing both the gas phase and one solid phase is considered. The method developed by Delhaye [6] is used to derive local instantaneous balance equations for both phases, chemical species continuity equations, and associated jump conditions at the solid-gas interface. At this step, the physicochemical processes of drying and pyrolysis due to the

Effective exchange coefficients and source terms in the generic transport equation for ϕ

Transport of	ϕ	Γ_ϕ	S_ϕ
Mass	1	1	$\sum_{k=1}^{N} \left[\dot{M}_k\right]_{Ik}$
x-momentum	u	μ	$-\rho g_x - \sum_{k=1}^{N} [F_{kx}]_{Ik} + \frac{\partial}{\partial x}(-\alpha_g p_g) + \frac{\partial}{\partial x}\left[\frac{1}{3}\alpha_g \mu \left(\frac{\partial u}{\partial x} - 2\frac{\partial v}{\partial y}\right)\right] + \frac{\partial}{\partial y}\left[\alpha_g \mu \left(\frac{\partial v}{\partial x}\right)\right]$
y-momentum	v	μ	$-\rho g_y - \sum_{k=1}^{N} [F_{ky}]_{Ik} + \frac{\partial}{\partial x}\left[\alpha_g \mu \left(\frac{\partial u}{\partial y}\right)\right] + \frac{\partial}{\partial y}(-\alpha_g p_g) + \frac{\partial}{\partial y}\left[\frac{1}{3}\alpha_g \mu \left(\frac{\partial v}{\partial y} - 2\frac{\partial u}{\partial x}\right)\right]$
Enthalpy	h	μ/Pr	$\frac{\partial}{\partial t}(\alpha_g p_g) - Q_{rad} - \sum_{k=1}^{N} [Q_{cond}]_{Ik} + \sum_{k=1}^{N} \left[\dot{M}_k e\right]_{Ik}$
Species i	Y_i	μ/Sc	$\sum_{k=1}^{N} \left[\dot{M}_k Y_i\right]_{Ik} + \dot{\omega}_i$

Note. The subscript Ik refer to the interface gas — solid interface.

thermal decomposition of the solid fuel are explicitly introduced. Char combustion appears implicitly through the jump conditions.

The second step is devoted to the formulation of multiphase ($k > 1$), reactive, and radiative field equations. Macroscopic balance equations are obtained from the local instantaneous equations by using the well-known formal averaging method. This method was first introduced by Anderson and Jackson [7], and used later by Gough and Zwarts [8] in a slightly different form. In this method, a weighting function is defined to obtain the average values of properties. Following Anderson and Jackson, a weighting function is defined that depends on spatial coordinates only. An averaged directional equation of the radiative intensity for the multiphase medium is similarly derived.

The equations of solid phases are strongly coupled to the gas-phase equations through exchange terms of drag, heat transfer, and chemical heterogeneous reactions. Moreover, a radiative transfer equation based on the P1-approximation is established to describe radiation in the fuel bed along with Markstein's model in the gas phase.

The chemistry including drying, and pyrolysis processes, combustion in the gas-phase, and surface combustion of char along with radiative transfer from the flame to the fuel particles are considered.

2.1. Gas-phase equations

The equation for the gas phase can be written in compact form using a dependent variable ϕ as follows:

$$\frac{\partial}{\partial t}(\rho\phi) + \frac{\partial}{\partial x}(\rho\phi u) + \frac{\partial}{\partial y}(\rho\phi v) = \frac{\partial}{\partial x}\left[\alpha_g \Gamma_\phi \left(\frac{\partial \phi}{\partial x}\right)\right] + \frac{\partial}{\partial y}\left[\alpha_g \Gamma_\phi \left(\frac{\partial \phi}{\partial y}\right)\right] + S_\phi \quad (3)$$

where $\rho = \alpha_g \rho_g$.

This equation describes mass continuity when ϕ stands for 1, momentum conservation when ϕ stands for the velocity components u and v, energy conservation when ϕ stands for the static enthalpy h, species conservation when ϕ stands for the mass fraction of the i-th species Y_i, $i = 1, nesp$, where $nesp$ is the number of species in the gas phase. The effective exchange coefficient of ϕ and source term, Γ_ϕ and S_ϕ, respectively, are given in Table.

Here p_g is the gas pressure, μ the gas dynamic viscosity, Pr and Sc the Prandtl and Schmidt numbers, g_x and g_y the components of the gravity acceleration in the x and y directions.

2.2. Equations for solid phase k ($k = 1$ to N)

2.2.1. Mass equation. The mass balance equation for solid phase k can be written as

$$\frac{\partial}{\partial t}(\alpha_k \rho_k) = -\left[\dot{M}_k\right]_{Ik}. \quad (4)$$

The rate of particle mass reduction relative to the thermal degradation of solid phase k can be represented by the sum of the mass rates $\dot{m}_k^{\mathrm{H_2O}}$, $\dot{m}_k^{pyr}$, and $\dot{m}_k^{char}$ due to water vaporization, pyrolysis, and char combustion, respectively:

$$\left[\dot{M}_k\right]_{Ik} = \dot{m}_k^{pyr} + \dot{m}_k^{\mathrm{H_2O}} + \dot{m}_k^{char}. \quad (5)$$

During drying and pyrolysis processes, the volume occupied by the solid phase is assumed to remain constant (α_k = const), and the mass equation reduces to

$$\alpha_k \frac{\partial \rho_k}{\partial t} = -\dot{m}_k^{pyr} - \dot{m}_k^{\mathrm{H_2O}} \quad (6)$$

while, during char combustion, the solid-phase density is assumed to remain constant (ρ_k = const), and the mass equation reduces to

$$\rho_k \frac{\partial \alpha_k}{\partial t} = -\dot{m}_k^{char}.$$

2.2.2. Momentum equation. Particles are assumed to be fixed in time and space. Hence, the assumption of motionless particles serves as momentum equations for the solid phase: $u_k = v_k = 0$.

2.2.3. Energy equation. By considering the assumption that fuel particles are thermally thin, i. e., the temperature throughout any solid particle is uniform while it is being heated, the solid-phase heat-conduction equation reduces to

$$\alpha_k \rho_k c_{p,k} \frac{\partial T_k}{\partial t} = -\dot{m}_k^{pyr} L^{pyr} - \dot{m}_k^{char} L^{char} - \dot{m}_k^{H_2O} L^{vap} + [Q_{cond}]_{Ik} + [Q_{rad}]_{Ik} + \left[Q_{rad}^{flame}\right]_{Igf} \quad (8)$$

where $c_{p,k}$ is the specific heat of solid phase k, subscript Igf refers to interface gas — fuel bed.

In this equation, $[Q_{cond}]_{Ik}$ represents the conductive/convective energy flux between the gas and solid phase k, $[Q_{rad}]_{Ik}$ represents the radiative energy flux between particles of the same phase k, and $\left[Q_{rad}^{flame}\right]_{Igf}$ represents the radiative energy flux from the flame to the particles at the top of the fuel bed. They will be expressed later.

Water vaporization and pyrolysis are endothermic processes ($L^{vap} = 2.25 \cdot 10^6$ J/kg and $L^{pyr} = 418$ J/kg) and char combustion is highly exothermic ($L^{char} = -1.2 \cdot 10^7$ J/kg).

2.3. Radiative transfer equation in the fuel bed

Radiative intensity I is deduced from the P1-approximation derived in detail in the paper of Larini et al. [3]

$$\frac{\partial}{\partial x}\left[\frac{\alpha_g}{3a_R}\frac{\partial}{\partial x}(\alpha_g I)\right] + \frac{\partial}{\partial y}\left[\frac{\alpha_g}{3a_R}\frac{\partial}{\partial y}(\alpha_g I)\right] = \sum_{k=1}^{N} [Q_{rad}]_{Ik} \quad (9)$$

where the global absorption coefficient is given by $a_R = \sum_{k=1}^{N} a_k$ and $[Q_{rad}]_{Ik} = a_k (I - 4\sigma T_k^4)$.

For spherical particles, $a_k = n_k \pi r_k^2$.

2.4. Equations of state

Enthalpy is defined to include the chemical energy

$$h(Y_s, T, P) = \sum_{s=1}^{nesp} Y_s \left(\Delta h_{fs}^0 + \int_{T_0}^{T} c_{p,s}(T)\, dT\right). \quad (10)$$

It appears clearly that any chemical composition variation (due to chemical reaction) implies enthalpy variations.

The equation of state for a multicomponent system based on ideal-gas assumptions can be written as

$$p = \rho R T \sum_{s=1}^{nesp} \frac{Y_s}{W_s} \quad (11)$$

where W_s is the molecular weight of the species s.

2.5. Combustion model in gaseous phase

As suggested by Grishin [9], the composition of the pyrolysis products is complicated (C, CO, CO_2, H_2O, CH_4, H_2, C_2H_6 ...), and one of the most representative components is CO. Therefore, the kinetic scheme is simplified by assuming that pyrolysis products are an effective gas of the CO type.

The combustion process is represented as a single, one-step reaction: fuel + oxydant $\Rightarrow$ products.

If the fuel is CO, fuel-rich condition ($n_{CO} > 2n_{O_2}$) or fuel-lean condition ($n_{CO} \leq 2n_{O_2}$) can occur locally:

$$n_{CO}CO + n_{O_2}O_2 = \begin{cases} 2n_{O_2}CO_2 + (n_{CO} - 2n_{O_2})\,CO \\ \qquad\qquad \text{(fuel —rich condition)} \\ n_{CO}CO_2 + (1/2)\,(2n_{O_2} - n_{CO})\,O_2, \\ \qquad\qquad \text{(fuel —lean condition).} \end{cases}$$

Then, the mass rate of production of gaseous species due to the above reaction can be easily determined from

$$\dot{\omega}_{CO} = -\frac{\rho}{\Delta t}\min\left(Y_{CO}, \frac{Y_{O_2}}{s_2}\right), \qquad \dot{\omega}_{O_2} = s_2 \dot{\omega}_{CO}, \qquad \dot{\omega}_{CO_2} = -(1 + s_2)\,\dot{\omega}_{CO} \quad (12)$$

where s_2 is the stoichiometric ratio of the chemical reaction and Δt is the hydrodynamic time step.

2.6. Mass rates due to thermal degradation of solid phase k

As suggested by Grishin [2], the rates of mass due to drying, pyrolysis, and char combustion can be deduced from the following Arrhenius-type laws:

$$\dot{m}_k^{H_2O} = 6 \cdot 10^5 T_s^{-1/2} p_k^{H_2O} \alpha_k \rho_k \exp(-6000/T_k),$$
$$\dot{m}_k^{pyr} = 3.63 \cdot 10^4 p_k^{pyr} \alpha_k \rho_k \exp(-9400/T_k), \quad (13)$$
$$\dot{m}_k^{char} = \frac{1}{s_1} 430 A_k \rho_{O_2} \exp(-9000/T_k)$$

where p_k^{pyr}, and $p_k^{H_2O}$ are the initial percentage of pyrolysis products and moisture content of the particle of solid phase k, and s_1 the stoichiometric ratio of the heterogeneous reaction.

Char is here idealized as pure carbon and the heterogeneous reaction is assumed to be $C+O_2 \Rightarrow CO_2$ ($s_1 = 8/3$).

2.7. Drag coefficient

The drag force per unit volume acting on the solid-phase particles can be expressed as

$$[\mathbf{F}]_{Ik} = \frac{1}{8} A_k C_{Dk} \rho |\mathbf{u}| \mathbf{u}. \qquad (14)$$

The particle drag coefficient C_{Dk} depends on the Reynolds number Re_k of solid phase k. For the present calculations, the correlation proposed in [10], valid for $\mathrm{Re}_k \leq 800$, is adopted

$$C_{Dk} = \frac{24}{\mathrm{Re}_k}\left(1 + 0.15\mathrm{Re}_k^{0.687}\right) \qquad (15)$$

where Re_k is defined in terms of the radius r_k of a particle of type k as $\mathrm{Re}_k = 2\rho_g |\mathbf{u}| r_k/\mu$.

The gaseous phase viscosity depends on temperature and is estimated from the viscosity of the various species s ($s = 1, nesp$) composing this phase

$$\mu(T) = \left(\frac{T}{T_{ref}}\right)^{0.75} \sum_{s=1}^{nesp} \mu_s(T_{ref}) Y_s \qquad (16)$$

where $T_{ref} = 302$ K.

2.8. Heat transfer coefficient

The convective/conductive heat flux between the gas phase and solid phase k is defined as

$$[Q_{cond}]_{Ik} = A_k h_k (T - T_k) \qquad (17)$$

where the heat transfer coefficient is deduced from the Nusselt number Nu_k of solid phase k and the thermal conductivity of the gas, λ, as $h_k = 0.5\lambda \mathrm{Nu}_k / r_k$.

Following Albini [11], a value of 0.35 for the Nusselt number has been used. It should represent well such fuels as conifer foliage and many grasses.

2.9. Radiative heat lost by the gas phase

The empirical model of Markstein [12, 13] is used. In this model, the radiative heat lost by an elementary flame volume is proportional to the rate of combustion in this volume, i. e.,

$$(Q_{rad})_{I,J} = \chi H_{comb} (\dot{\omega}_{CO})_{I,J} \qquad (18)$$

where χ is a constant that depends on the nature of the fuel and H_{comb} the heat released by the combustion. A value of $\chi = 0.35$ means that 35 % of the energy released by the combustion is lost by radiation to the environment.

A part of this energy lost by radiation is transferred to the top of the fuel bed, namely,

$$\left[Q_{rad}^{flame}\right]_{Igf} = \sum_{all\ gas\ volume\ I,J} (Q_{rad})_{I,J} (F_{view})_{I,J} \qquad (19)$$

where $(F_{view})_{I,J}$ is the radiation shape factor defined as the fraction of energy leaving the gas volume (I, J) that reaches a fuel bed surface element (Fig. 3).

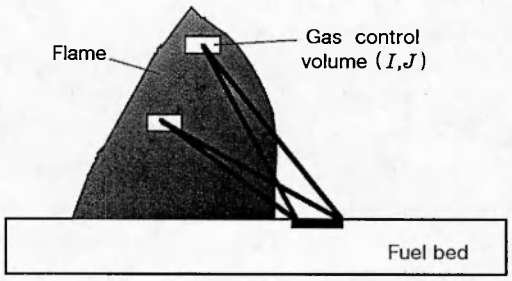

Fig. 3. Schematic of the radiation model from the flame cells to the top of the fuel bed

3. NUMERICAL METHOD

The governing equations are discretized on a staggered non-uniform grid using a finite-volume procedure with a hybrid difference scheme for the convective terms [14] and a second order backward Euler scheme for temporal discretization. A brief description on the method is given below.

The generic transport equation and the radiative transfer equation associated with adequate boundary conditions can be reduced to an algebraic equation. For cell P in Fig. 4,

$$\left[3(\rho_P \phi_P)^{n+1} - 4(\rho_P \phi_P)^n + (\rho_P \phi_P)^{n-1}\right] \frac{\Delta x \Delta y}{2\Delta t} = -J_e + J_w - J_n + J_s + S_\phi^{n+1} \Delta x \Delta y \qquad (20)$$

with

$$J_i = \left[\rho u_i \phi_i - \Gamma_\phi \left(\frac{\partial \phi}{\partial x_j}\right)_i\right] \Delta_i, \quad i = e, w, n, s \qquad (21)$$

where Δt is the time step, the superscripts n, $n+1$, and $n-1$ refers to values at times $t + \Delta t$, t, and $t - \Delta t$, and u_i and Δ_i are respectively the normal velocity and the transverse grid size at

interface i between two contiguous control volumes. The evaluation of interface flux between two finite volumes (J_i) depends on the choice of a numerical scheme. It is constituted by two contributions which represent the two modes of transport by convection and molecular diffusion. The diffusion term is generally discretized using second-order central-difference scheme. The same approach could not be used to calculate convective terms because of the growth of unphysical oscillations and instabilities generated as the cell Peclet number (see the definition below) is greater than 2. The alternative solution to avoid this oscillatory behavior consists in approximating the convective flux by using first-order upwind schemes: Upwind, Power Law, and Hybrid shemes [14]. In this case, the flux of the unknown quantity at each interface is evaluated from the following expression (at the east interface for example)

$$J_e = F_e\phi_P + D_e A(P_e)(\phi_P - \phi_E) \qquad (22)$$

with

$$F_e = (\rho u)_e \Delta y, \quad D_e = (\Gamma_\phi)_e \Delta y/\Delta x_e \qquad (23)$$

where $P_e = F_e/D_e$ is the cell Peclet number and Δx_e the distance between points P and E in Fig. 4.

In this work, the hybrid scheme is used. It corresponds to the following definition of the function A:

$$A(P_e) = \max(0, 1-0.15|P_e|) + \max(0, -P_e). \qquad (24)$$

The resulting systems of linear algebraic equations for each variable is then solved in turn by an iterative solver such as the line-by-line tridiagonal matrix algorithm [14]. In addition, to procure convergence and prevent low-frequency behavior of the solution typical of this type of buoyancy-driven flow [15], all the variables were under-relaxed using inertial relaxation [14]. Under-relaxation is a very useful device to avoid divergence in the iterative solution of strongly nonlinear algebraic equations. This process is used to slow down changes, from iteration to iteration, in values of the dependent variables. In our study, the inertia was taken to be 0.7.

The PISO non-iterative method developed by Issa et al. [16] is used for computing the solution of the time-dependent, implicitly discretized fluid flow equations by operator splitting. In this segregated solution algorithm, a predictor-corrector procedure is used for the solution of flow equations in terms of primitive variables. In the predictor step, the momentum equations are solved using a pressure field determined by previous iteration. The resulting velocity field will not, in general, satisfy the continuity equation. Corrections to the velocity and pressure fields are obtained by solving a pressure correction which is derived from the momentum and continuity equations. The PISO algorithm is an improvement of the well-known SIMPLE (Semi-Implicit Method for Pressure Linked Equations) algorithm developed by Patankar and Spalding [17]. The SIMPLE algorithm and its variants has been widely used throughout the computational fluid dynamics community and has been used extensively in the simulation of fires (see, for example, [18]).

Different grids were tested to ensure that the solution was independent of the grid density. A grid size of 6300 cells (90 × 70) has been used for all of the cases solved.

4. RESULTS AND DISCUSSION

The multiphase model described above has been employed to describe the behavior of a spreading wildfire through a 0.04-m litter of dead

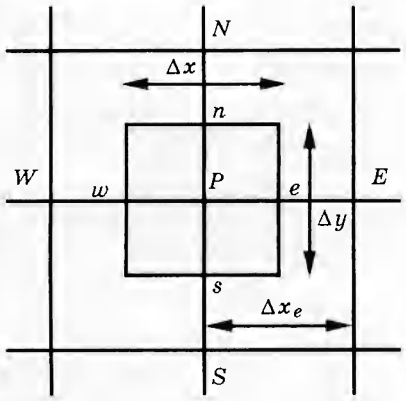

Fig. 4. Representative scalar control volume

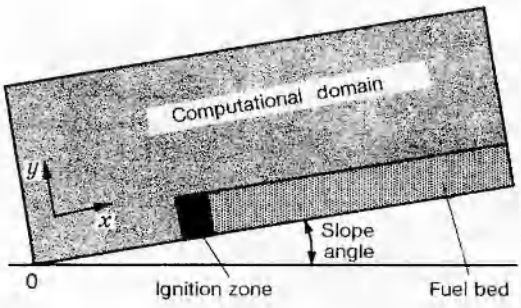

Fig. 5. Definition sketch of the calculation domain showing the ignition zone and the fuel bed

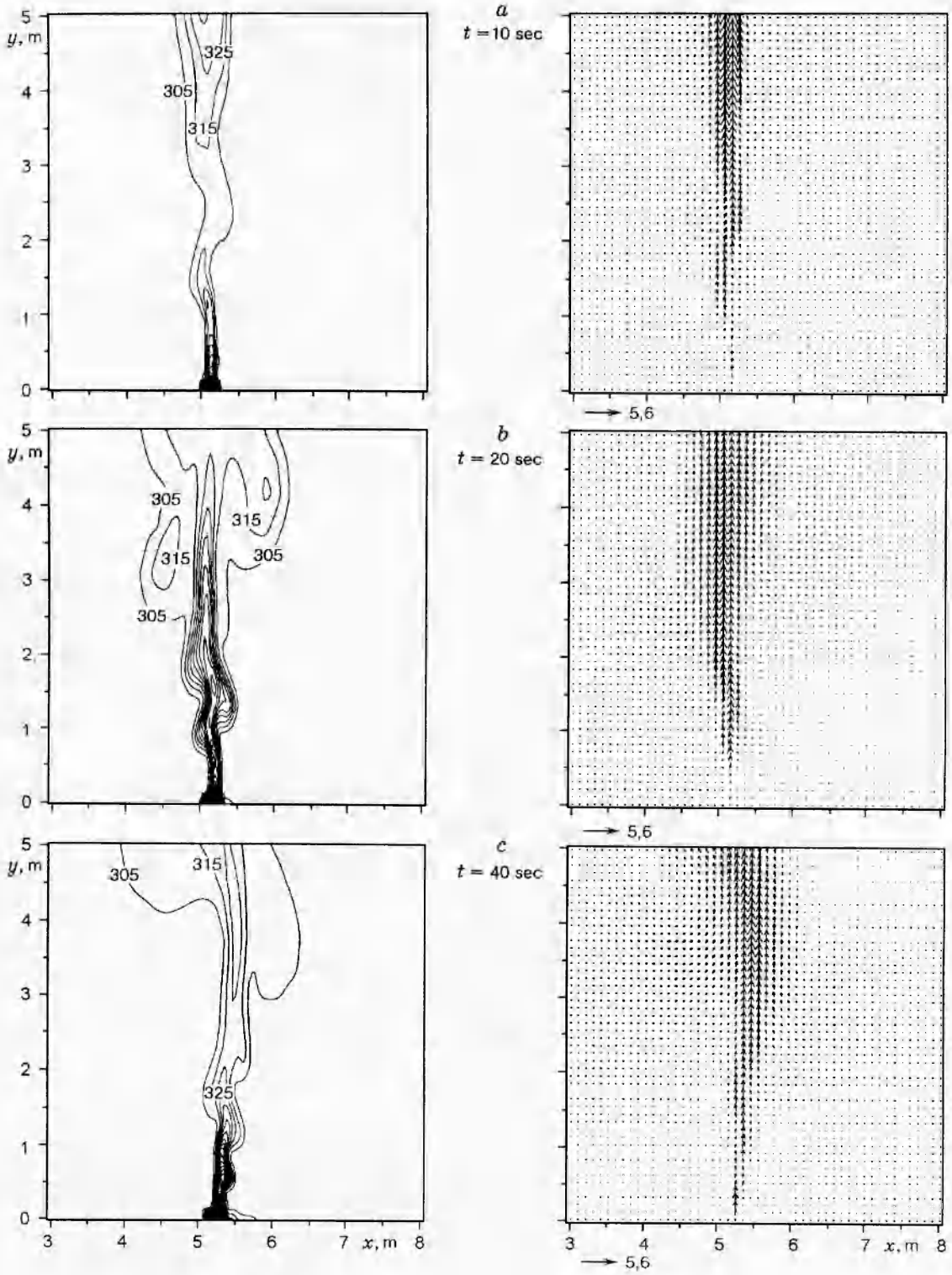

Fig. 6. A closer view of the gas temperature contours and velocity vectors at times 10, 20, 40, 60, 80, and 100 sec

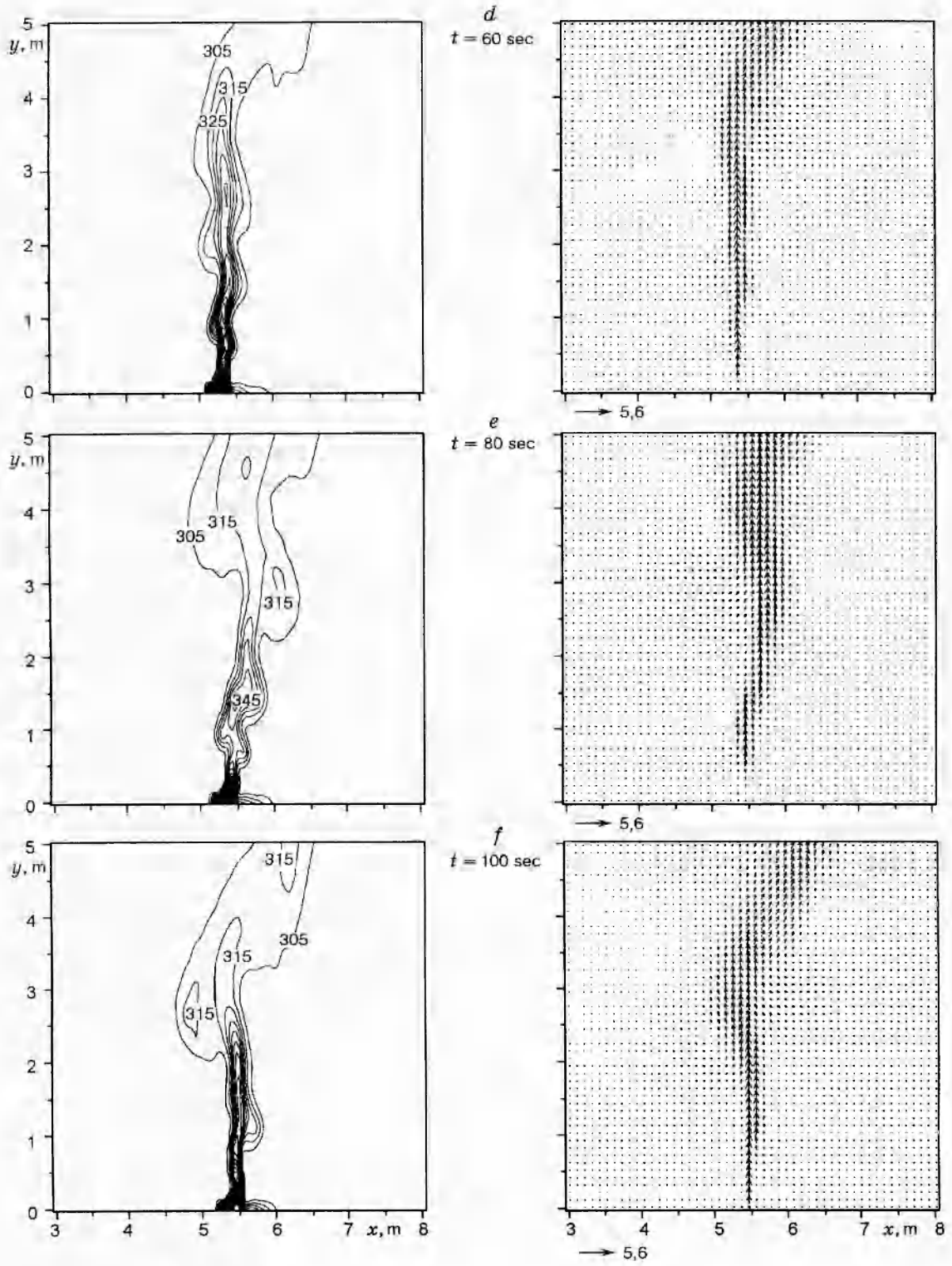

Fig. 6 (continued)

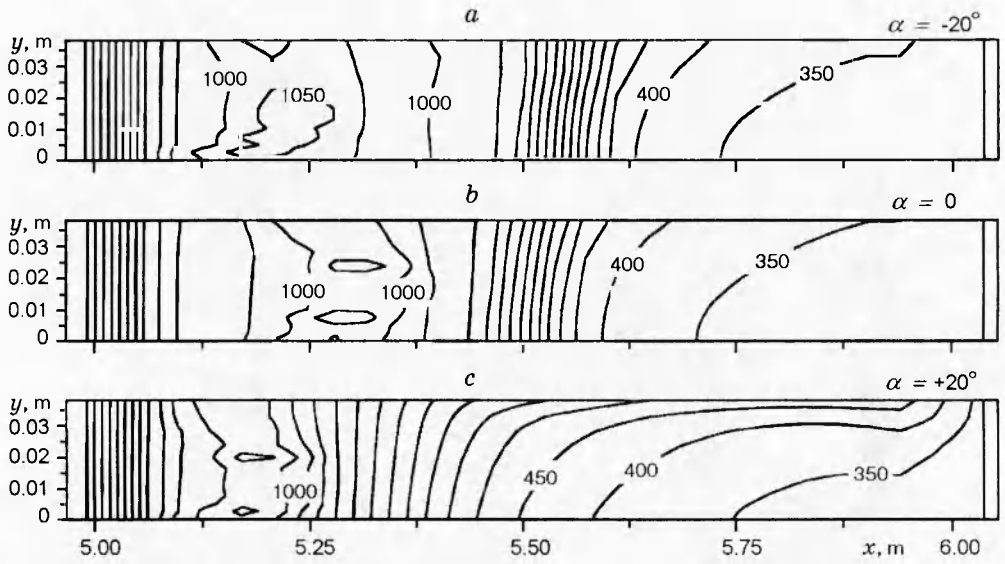

Fig. 7. A closer view of the solid-phase temperature contours for different slopes angle α

coniferous needles (Pinus Pinaster). A definition sketch of the rectangular calculation domain is shown in Fig. 5. In such a problem, the free boundaries of the computational domain have to be located far enough from the source so as not to disturb the solution. However, for reducing computational time and memory demand, numerical tests have been performed in order to determine the optimum dimensions of the solution domain. In the present study, a domain 15 m high and 11 m long was found to be satisfactory for a fuel bed depth of 0.04 m.

Test conditions used in the present work are the same as those used for laboratory experiments conducted by Dupuy [19], where used a device composed of a plate which was 1.70 m long and 0.59 m wide (1 m^2). In this experimental study, the effects of slope on fire behavior for different levels of fuel load are investigated.

In accordance with this study, the measured surface-to-volume ratio and density of the needles were, respectively, 4550 m^{-1} and 680 kg/m^3. The initial moisture content was 2 %. Therefore, the fuel to be burned is distributed uniformly throughout a layer of constant thickness of 0.04 m to give a loading density of 0.8 kg/m^2.

The line fire is ignited at 5.03 m from the left boundary of the computational domain over a distance of 0.14 m. In this ignition zone (Fig. 5), the fuel temperature varies linearly from 300 to 1200 K until 15 sec.

Due to the large computing time, computations are stopped either after 100 sec or when the front of pyrolysis has covered a distance of 0.6 m.

4.1. Line fire spreading on a flat terrain

Figure 6 shows closer views of the gas temperature and velocity fields at times 10, 20, 40, 60, 80, and 100 sec. They reveal the unsteady stages of the wildfire propagation and the development of a strong buoyant plume with entrained vortices. Temperature varies from 300 to 1100 K.

The upward movement of the flame gases is mainly due to buoyancy effects, as usually observed in natural fires. The velocity fields confirm the low flow rate of the fuel vapor above the fuel bed and, hence, the associated momentum has no significant effect on flame behaviour which explains its nonordered structure. Moreover, the shear forces induce instability in the gas flow which leads to flame flickering as confirmed by the variable density of the isotherm curves in Figs. 6,*b–f*. One can notice the succession of pulses on both sides of the fire plume.

The solid-phase temperature in the fuel bed at $t = 100$ sec is shown in Fig. 7,*b*. The maximum of temperature is obtained in the region where char combustion occurs (at about $x = 5.30$ m), while the maximum gas temperature is observed in the intense pyrolysis region (at about $x = 5.45$ m). This confirms the necessity of accounting for thermal nonequilibrium between the phases. Isotherms are nearly vertical with the exception of the region of unburnt heated zone (from $x = 5.48$ m) where the top of the fuel bed is first heated.

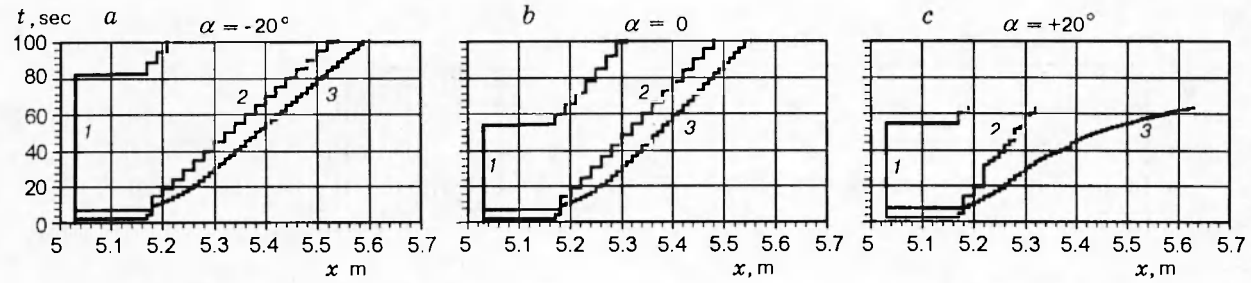

Рис. 8. Front trajectories for different slopes angle α:
1 — ash formation front, *2* — char combustion front, *3* — pyrolysis front

In Fig. 8,*b*, the trajectories of the fronts of pyrolysis, char combustion (end of pyrolysis), and ash (end of char combustion) are plotted. As clearly seen, steady-state solution seems to be reached from $t = 60$ sec, since the distance between two successive fronts remains nearly constant. On the left-hand side of the bed, ash formation begins at about $t = 54$ sec.

4.2. Slope effects

The final fields of gas temperature and velocity are given in Figs. 9,*a*–*c* for different slopes: −20, 0, and +20°. A more important distortion of the fire plume is observed for downslope fire (Fig. 9,*a*). Because of the downslope, a part of the hot gases produced by the pyrolysis product oxidation travels through the char combustion region, leading to an enlargment of the burning zone and a higher gas temperature level. For upslope fire (Fig. 9,*c*), as pointed out by Zukosky [20], it is surprising that the hot gas plume and the flame stay attached to the surface and do not rise vertically above the source of the heat. This attachment, which is well-known to be more pronounced in 2D than in 3D flows, seems to be due to the pressure field induced by the entrainment of air into the plume.

Examination of particle isotherms (Fig. 7) shows an increase in the combustion zone as slope increases from −20 to +20°. For upslope configuration (Fig. 7,*c*), in the heated unburnt fuel region, a deeper penetration of the thermal wave due to flame radiation can be observed, as illustrated by the curvature of the isotherms in Fig. 7,*c* (see, for example, isotherm 400 K).

Front trajectories are plotted in Fig. 8 for different slopes. It appears clearly that, unlike downslope (Fig. 8,*a*) and noslope (Fig. 8,*b*) fires, the steady-state solution has not been reached for upslope fire (Fig. 8,*c*). From an experimental point of view, as observed by Dupuy [19], for Pinus Pinaster litters, fires were not steady as soon as slope exceeds a value of 10°. This must be connected with what was reported by Byram et al. [21] and Weise [22] on unsteady spread in relation with too short fuel beds. The change in curvature of front 1 for upslope (Fig. 8,*c*) expresses the acceleration of the pyrolysis front; the steady-state solution should require a longer distance of propagation. As previously mentioned, the enlargment of the char combustion zone (between fronts *2* and *3*) is evident in Figs. 8,*a*,*b*.

4.3. Comparison with experiments

In Fig. 10, computed rates of propagation for slope angles of −20°, 0, and +20° are compared with those obtained from experiments [19]. The experimental values (min and max) are deduced from three replications done for each slope. The agreement is very good, and slope effects are well represented.

5. CONCLUSIONS

A 2D multiphase radiative and reactive model of line fire propagation has been performed. It accounts for the hydrodynamic aspects of the flow and the basic physicochemical processes of thermal degradation (heating, drying, pyrolysis, and combustion) and uses first-order Arrhenius kinetics to describe thermal degradation and combustion. It models the development of a line fire from the moment of initiation to quasi-steady propagation.

The first results obtained using the 2D multiphase model are very encouraging. They do not only give a faithful reproduction of slope effects on the wildfire behaviour but they also lead to realistic rates of propagation.

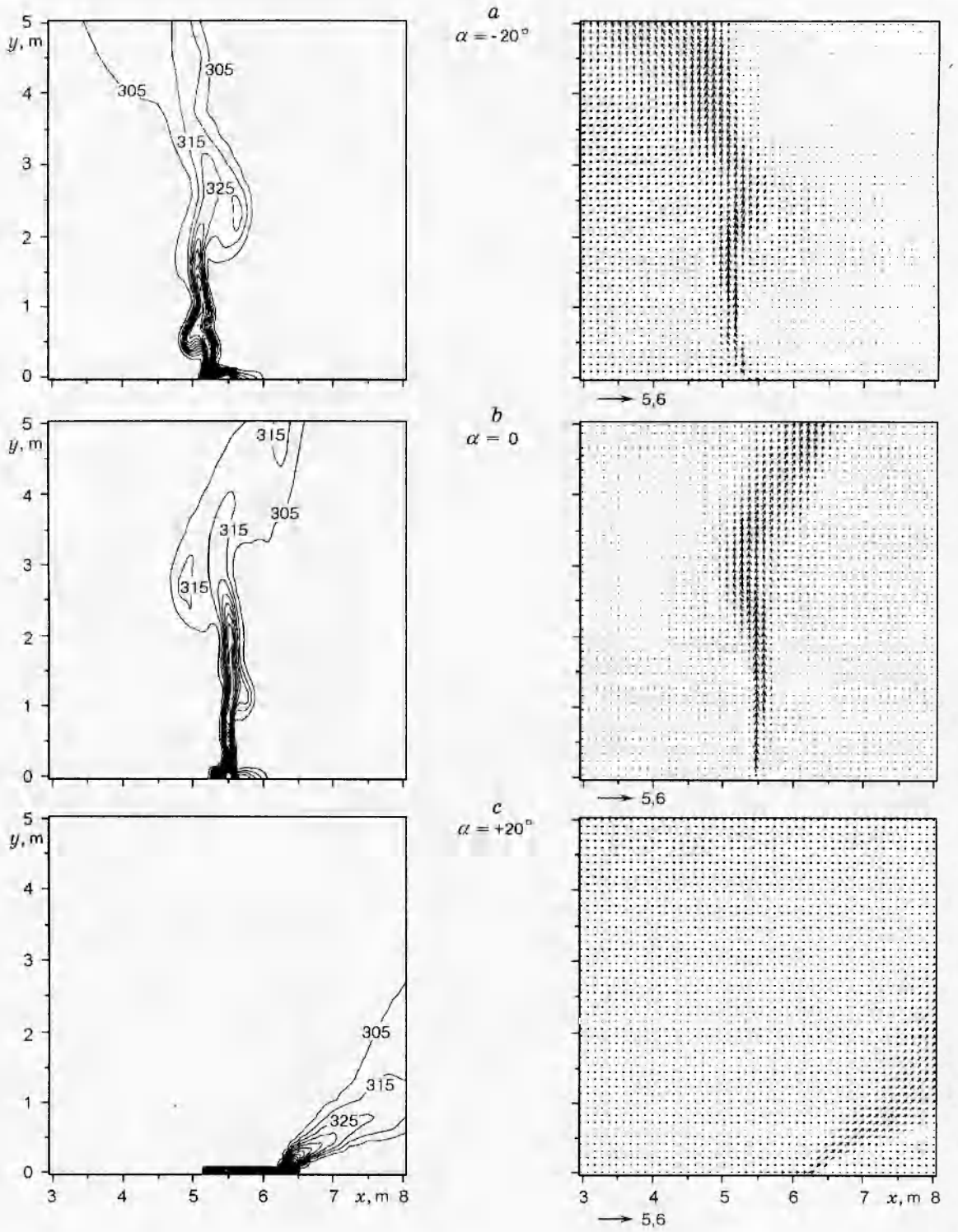

Fig. 9. A closer view of the final gas temperature contours and velocity vectors for different slopes

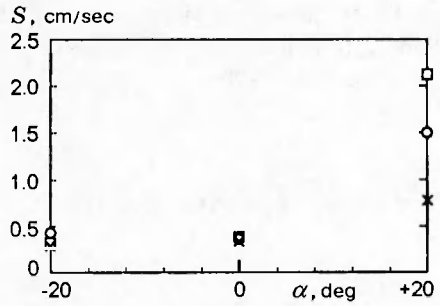

Fig. 10. Rate of spread (S) versus slope α. Min (×) and max (□) experimental values for three replications are plotted (○ — multiphase model)

A more refined model including modeling of soot formation and turbulence is being developed to improve the radiation model.

Therefore, more sophisticated models or simulations are not warranted until reliable information on drag, heat transfer, and physicochemical process of thermal degradation is available. Specific experiments are needed for obtaining such information and measuring turbulence and soot quantities as well as data from real fires.

AKNOWLEDGMENT

The European Economic Commission is gratefully acknowledged for providing partial funding for this research in the frame of the EFAISTOS Project.

REFERENCES

1. **Albini F. A.** A model for fire spread in wildland fuels by radiation // Combust. Sci. Techol. 1985. V. 42. P. 229–258.
2. **Grishin A. M., Gruzin A. D., Zverev V. G.** Study of the structure and limits of propagation of the front of an upstream forest fire // Fizika Goreniya i Vzryva. 1985. V. 21, N 1. P. 11–21.
3. **Larini M., Giroud F., Porterie B., Loraud J. C.** A multiphase formulation for fire propagation in heterogeneous combustible media // Int. J. Heat Mass Transfer. 1998. V. 41, N 6-7. P. 881–897.
4. **Weber R. O.** Modeling fire spread through fuel beds // Prog. Energy and Combust. Sci. 1991. V. 17. P. 67–82.
5. **Grishin A. M., Gruzin A. D., Zverev V. G.** Mathematical modeling of the spreading of high-level forest fires // Sov. Phys. Dokl. 1983. V. 28. P. 328–330.
6. **Delhaye J. M.** Local instantaneous equations — instantaneous space — averaged equations — two-phase flows and heat transfer // Proc. NATO Advanced Study Institute, Istambul. 1976. V. 1.
7. **Anderson T. B., Jackson R.** A fluid mechanical description of fluidized bed // Ind. Eng. Chem. Fundam. 1967. V. 6. P. 527–539.
8. **Gough P. S., Zwarts F. J.** Modeling heterogeneous two-phase reacting flow // AIAA J. 1979. V. 17. P. 17–25.
9. **Grishin A. M., Zverev V. G., Shevelev S. V.** Steady-state propagation of top crown forest fires // Fizika Goreniya i Vzryva. 1986. V. 22, N 6. P. 101–108.
10. **Clift R., Grace J. R., Weber M. E.** Bubbles, Drops, and Particles. New York: Academic Press, 1978.
11. **Albini F. A.** Wildland fire spread by radiation — a model including fuel cooling by natural convection // Combust. Sci. Technol. 1986. V. 45. P. 101–113.
12. **Markstein G. H.** Scaling of radiative characteristics of turbulent diffusion flames // Proc. (Intern.) 16th Symp. on Combustion. Pittsburgh, PA: The Combustion Inst., 1977. P. 1407–1419.
13. **Markstein G. H.** Relationship between smoke point and radiant emission from buoyant turbulent and laminar diffusion flames // Proc. 20th Symp. on Combustion. Pittsburgh, PA: The Combustion Inst., 1985. P. 1055–1061.
14. **Patankar S. V.** Numerical Heat Transfer and Fluid Flow. New York: McGraw Hill, 1980.
15. **Moss J. B.** Turbulent diffusion flames // Combust. Fundamentals of Fire / G. Cox (Ed.). San Diego, CA: Academic Press, 1995.
16. **Issa R. I., Ahmadi-Befrui B., Beshay K. R., Gosman A. D.** Solution of the implicitly discretized reacting flow equations by operator-splitting // J. Comp. Phys. 1991. V. 93. P. 388–410.
17. **Patankar S. V., Spalding D. B.** A calculation procedure for heat, mass, and momentum transfer in three-dimensional parabolic flows // Int. J. Heat Mass Transfer. 1972. V. 15.
18. **Cox G.** Compartment fire modeling // Combust. Fundamentals of Fire / G. Cox (Ed.). San Diego, CA: Academic Press, 1995.
19. **Dupuy J. L.** Slope and fuel load effects on fire behavior: laboratory experiments in pine needle fuel beds // Int. J. Wildland Fire. 1995. V. 5. P. 153–164.
20. **Zukosky E. E.** Properties of fire plumes // Combust. Fundamentals of Fire / G. Cox (Ed.). San Diego, CA: Academic Press, 1995.

21. **Byram G. M., Clement H. B., Elliot E. R., George P. M.** An Experimental Study of Model Fires. U.S. Forest Service, Southeastern Forest Exp. Station, Tech. Report 3, 36. 1964.

22. **Weise D. R.** Modeling Wind and Slope Induced Wildland Fire Behaviour: PhD Dissertation. Univ. of California, CA, 1993.

Поступила в редакцию 18/VII 1997 г.